

Fluctuations of the thermal fronts off northeastern Taiwan

Yi-Chia Hsin,¹ Tzu-Ling Chiang,¹ and Chau-Ron Wu¹

Received 19 February 2011; revised 24 June 2011; accepted 8 July 2011; published 5 October 2011.

[1] A high-resolution sea surface temperature (SST) data derived from several satellites is used to investigate the variability of the thermal front off northeastern Taiwan. Hidden by a dominant annual cycle, the SST data cannot reveal the thermal front fluctuation in the form of Hovmöller diagram. An innovative methodology has been applied to the SST satellite imagery to derive the SST Standardized Index (SSTSI), capable of revealing the frontal variability with multiple time scales. Principal component analysis shows that the SSTSI variation consists mainly of two modes. Mode 1 represents a strong annual cycle related to the seasonal reversal of the monsoonal winds. The temperature gradient is enhanced in winter and a cold dome is observed off northern Taiwan in summer. Mode 2 is highly correlated with the upstream Kuroshio variability. The shoreward (seaward) migration of the thermal front takes place when the Kuroshio transport weakens (strengthens). The results are consistent with transports estimated by tidal gauge measurements, satellite altimeter-based sea level anomaly, and surface flow patterns derived from high-frequency radars. Mode 2 is coherent with the Kuroshio transport through the East Taiwan Channel at periods of 120 and 45 d with a time lag of 40 and 11 d, respectively. This 120 d fluctuation is due to the interaction between westward-propagating eddies and the Kuroshio east of Taiwan, while the 45 d signal arises from the Kuroshio's self-instability. The interannual variations of the SST pattern in winter and summer are also discussed.

Citation: Hsin, Y.-C., T.-L. Chiang, and C.-R. Wu (2011), Fluctuations of the thermal fronts off northeastern Taiwan, *J. Geophys. Res.*, 116, C10005, doi:10.1029/2011JC007066.

1. Introduction

[2] A persistent oceanic front is observed off northeastern Taiwan, drawing much attention because of cross-frontal water exchange and enhanced bioproductivity in the region [Hickox *et al.*, 2000; Chen, 2009]. The front is associated with the Kuroshio and is strongly modulated by the Kuroshio variations on synoptic, seasonal, and interannual scales. The Kuroshio, a western boundary current in the North Pacific, is the main current off Taiwan. It carries large amounts of heat, salt, and mass poleward from the tropical ocean and plays an important role in the global climate [Qu, 2003]. Through the East Taiwan Channel (ETC) between Taiwan and Iriomote (see Figure 1a for locations), the Kuroshio enters the East China Sea (ECS), roughly following the continental slope around 200 m isobath to the northeast [Lie and Cho, 2002]. The Kuroshio water is present as a warm tongue in the ECS, and forms a distinct thermal front off northeastern Taiwan extending northeastward to the southern Japan. Especially in winter, the front is much more obvious because of the contrast between the cold shelf water and the warm Kuroshio.

[3] In summer, a cold dome with diameter of ~100 km is frequently observed near the shelf break off northeastern Taiwan. The feature is evident in the hydrographic and current data from field surveys and sea surface temperature (SST) images by satellites [e.g., Tang *et al.*, 2000; Tseng *et al.*, 2000; Belkin and Cornillon, 2003; Cheng *et al.*, 2009]. By statistical analysis using multisensor satellite data, Cheng *et al.* [2009] concluded that the cold dome is most frequently seen in June–October (>30% of time) with a maximum in July (54% of time), while the area of the cold dome is also the most expansive. The cold dome always appears accompanied with upwelling, bringing subsurface nutrient-rich water up to the sea surface, providing a major source of nutrients to the ECS [Chen, 1996]. Wu *et al.* [2008] further demonstrated that the occurrence of the cold dome is connected with the zonal migration of the Kuroshio off northeastern Taiwan. The seasonal Kuroshio migration, seaward in summer and shoreward in winter, is observed in the shipboard Acoustic Doppler Current Profiler (ADCP) velocity data and hydrographic data [Sun, 1987; Tang *et al.*, 2000; Liang *et al.*, 2003]. Recently, based on surface currents derived from high-frequency (HF) radars around the southern Ryukyu Islands, Ichikawa *et al.* [2008] also found that the Kuroshio is stronger in summer, and the faster (slower) Kuroshio velocity accompanies southward (northward) movement of the Kuroshio axis.

¹Department of Earth Sciences, National Taiwan Normal University, Taipei, Taiwan.

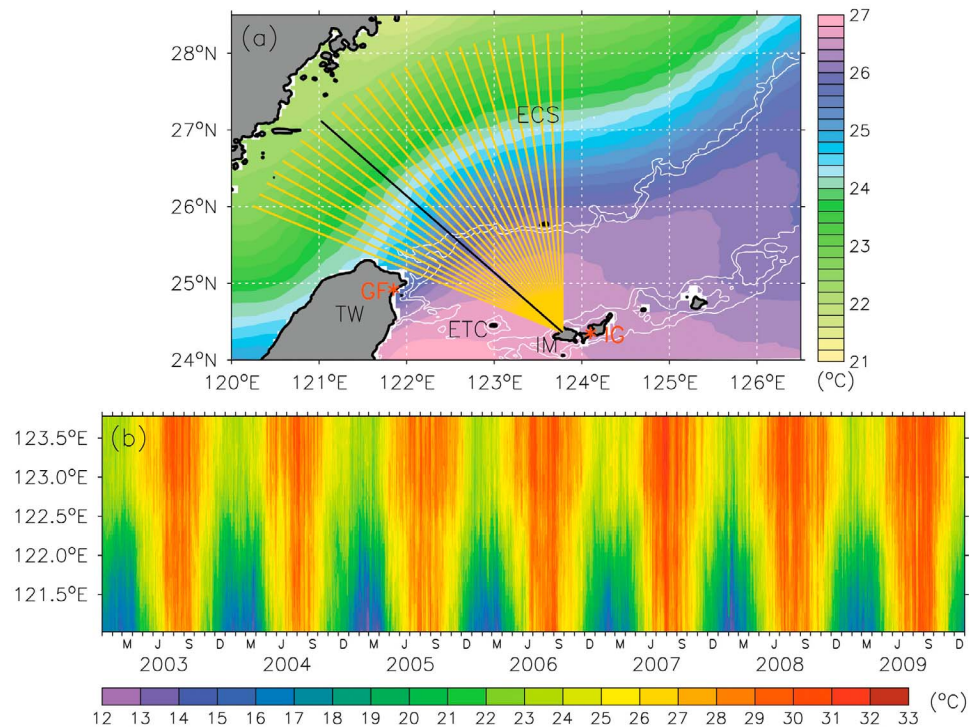


Figure 1. (a) Mean sea surface temperature (SST) (2003–2009) in the study area. Yellow lines in the fan-shaped domain are used for analyses. White contours are 200 m and 500 m isobaths. ECS, TW, ETC, IM, GF, and IG are the abbreviations of East China Sea, Taiwan, East Taiwan Channel, Iriomote, Genfang, and Ishigaki, respectively. The two red stars on GF and IG denote the positions of two tidal gauges used in this study. (b) Hovmöller diagram of SST along the black line in Figure 1a.

[4] Several studies have focused on the forcing mechanism of the seasonal Kuroshio variation off northeastern Taiwan. Using a wind-driven model, *Chao* [1991] attributed the seasonal migration to the monsoonal winds. In winter (summer), onshore (offshore) Ekman transport by the northeasterly (southwesterly) monsoon forces the surface Kuroshio shoreward (seaward). On the other hand, based on ADCPs moored on the continental slope off northeastern Taiwan, *Chuang and Liang* [1994] concluded that the northward Kuroshio intrusions coincided with the arrivals of cold air outbreaks in fall, which cool the surface water and generate dense water over the shelf region. The dense water spills off the shelf, cascading over the slope, and triggers on-shelf intrusion of the warmer Kuroshio water near the surface. In summer, the shelf water warms up and the shoreward Kuroshio intrusion ceases. Utilizing an idealized numerical model, *Oey et al.* [2010] further verified this idea and addressed a relevant dynamical process using the Joint Effect of Baroclinicity and Relief (JEBAR) effect. Besides, *Ichikawa et al.* [2008] related the surface flow variability to the Kuroshio meander east of Taiwan. They observed the Kuroshio axis in the southern ECS moves southward with an increase of speed after ~ 40 d when a seaward meander of the Kuroshio takes place off eastern Taiwan. In summary, the complicated circulation and its associated thermal front off northeastern Taiwan is largely modulated by the monsoon, surface cooling via the heat flux, and the Kuroshio fluctuation in the upstream region east of Taiwan.

[5] In this study, we use a high-resolution satellite SST imagery to investigate the variability of the Kuroshio thermal front off northeastern Taiwan, which is generated by the confrontation between the warm Kuroshio and cold shelf water. We propose an innovative methodology to explore the thermal front variations. The improved methodology has revealed the frontal variability on multiple time scales. The paper is structured as follows. Data and methodology are introduced in section 2. The results are described and discussed in section 3, and summarized in section 4.

2. Data and Methodology

2.1. Sea Surface Temperature

[6] The SST imagery used in the study is a high-resolution ($0.05^\circ \times 0.05^\circ$) daily product developed by the New Generation Sea Surface Temperature (NGSST) Development Group (<http://www.ocean.caos.tohoku.ac.jp/>). The product is objectively merged from two infrared radiometers (Advanced Very High Resolution Radiometer and Moderate Resolution Imaging Spectroradiometer) and one microwave radiometer (Advanced Microwave Scanning Radiometer–Earth Observing System). The spatial coverage of the NGSST ranges between 13° – 63° N and 116° – 166° E, and it is available after June 2002. The SST data between 2003 and 2009 are used for analysis.

[7] Furthermore, hidden by a strong annual cycle, the SST imagery cannot distinctly reveal the zonal movement of

the thermal front in the form of Hovmöller diagram (see Figure 1b). The SST-based Standardized Index (SSTSI) is then established as

$$\text{SSTSI}(s, t) = \frac{\text{SST}(s, t) - \text{SSTM}(t)}{\text{Max}(|\text{SST}(s, t) - \text{SSTM}(t)|)}, \quad (1)$$

here s is function of both longitude and latitude along each specified cross-frontal section shown as yellow lines (including black line) in Figure 1a, SSTM is the time-dependent mean value, and $\text{Max}(|\text{SST}(s, t) - \text{SSTM}(t)|)$ means the maximal absolute value of SST(s, t) minus SSTM(t) along each section. SSTSI ranges between -1 and 1 . Positive (negative) SSTSI denotes a warmer (colder) SST from the mean along the section at a time. The empirical orthogonal function (EOF) is implemented to further analyze SST images and SSTSI. To filter out high-frequency perturbations (or noises), a 30 d low-passed filter is adopted for SST images and SSTSI before applying EOF. Note that sections selected to calculate SSTSI have to be perpendicular to the front. We have tested several different areas around northern Taiwan, and all the results are robust as long as the selected sections are nearly perpendicular to the front. For convenience, we utilize the fan-shaped area with the apex on Iriomote (the yellow lines in Figure 1a) in this study.

2.2. Sea Level Data

[8] Comparing with velocity measurements by vessels or moorings, sea level records from tidal gauges provide a more economic and easier way to monitor water mass flux into the ECS. By correlating sea level anomaly difference between both sides of ETC with transport derived from mooring array, Yang *et al.* [2001] proposed several transport estimators to quickly calculate the ETC transport by tidal gauge measurements. In this study, equation (3) of Yang *et al.* [2001] is adopted to estimate the ETC transport using daily sea level measurements. The equation is as follows:

$$Q = 0.25 \times (h_{IG} - h_{GF}) + 20.87, \quad (2)$$

where Q is the transport (Sv) based on daily sea level anomaly difference (cm) between Ishigaki (h_{IG}) and Genfang (h_{GF}) (see Figure 1a for locations). The hourly sea level record at Ishigaki is obtained from the Joint Archive for Sea Level (JASL) (<http://uhslc.soest.hawaii.edu/uhslc/jasl.html>), in which obvious errors are corrected and gaps less than 25 h are interpolated linearly. The hourly sea level record at Genfang is provided by the Central Weather Bureau, Taiwan, available from May 1996 to April 2008 (<http://www.cwb.gov.tw/eng/index.htm>). The tidal-gauge-based transport estimates used in this study are calculated for the period between January 2003 and April 2008. Before calculating the ETC transport, a 48 h least squares Lanczos filter is used to remove the signals on the dominant tidal periods within 2 d. Obvious errors were removed from the 48 h low-passed time series. Finally, hourly data were averaged daily, and a 30 d low-passed filter is applied to the data.

[9] Another sea level data used in the study are from satellite altimeters. The sea level anomaly product is provided by Archiving, Validation, and Interpretation of Satellite Oceanographic data (AVISO) (<http://www.aviso.oceanobs.com/>), which is merged from multisatellite altimeter data of

the TOPEX/Poseidon, European Remote Sensing satellite 1 and 2 (ERS 1 and 2), Jason 1 and 2, Envisat, and Geosat Follow-On (GFO). The product is gridded on a Mercator grid of $1/3^\circ \times 1/3^\circ$ and a time interval of 7 d. It is available after October 1992.

3. Results and Discussions

3.1. Spatiotemporal Variability of SST

[10] Figure 1a presents the mean SST pattern averaged over 2003–2009. In general, the annual mean SST can be spatially divided into two parts by the continental slope (denoted by 200 m and 500 m isobaths), located in the ECS shelf and the Kuroshio region. In the shelf area, the SST contours are in general parallel to the isobaths. The SST in the Kuroshio region appears as a warm tongue with temperature decreasing toward the northeast. The largest difference of temperature between the shelf region and the Kuroshio area is about 6°C . Figure 1b shows the Hovmöller diagram of SST along a cross-frontal section between 27.1°N , 121.0°E and 24.4°N , 123.8°E (black line in Figure 1a). The seasonal variation is obvious. Because of the seasonal solar heating pattern of the northern hemisphere, the temperature is higher (up to $\sim 33^\circ\text{C}$) in summer and lower (down to $\sim 12^\circ\text{C}$) in winter. In longitudinal view, SST on the offshore side is higher than inshore regardless of season because the Kuroshio serves as a persistent source of warm water. The wintertime cooling of the shelf area enhances the temperature gradient in winter. Note that the horizontal movement of the Kuroshio front is not obvious in the time-longitude diagram of SST.

[11] The seasonal evolution of SST around northern Taiwan is further displayed in Figure 2. In order to be capable of seeing the SST distribution clearly, the color scale is properly adjusted from month to month. The difference between the maximum and minimum values of the color scales can be roughly regarded as the largest temperature difference between the shelf and the Kuroshio for the given month. The difference is larger in January and April ($\sim 9^\circ\text{C}$) (Figures 2a and 2b), and smaller in July and October ($\sim 3^\circ\text{C}$) (Figures 2c and 2d), indicating that the SST gradient is larger in winter and spring than in summer and fall. The SST distributions in January and April are quite similar to the annual mean pattern (Figure 1a), except for larger gradients in both the shelf and Kuroshio region. In July, a cold dome can be seen northeast of Taiwan. The cold dome becomes very weak and moves slightly shoreward in October, and disappears afterward in January and April. The timing and location of the cold dome's appearance agree well with the finding of Cheng *et al.* [2009], who found that the cold dome is on average the least often seen in January and most often seen in July. In July–October, the SST contours in the shelf region spread apart, which means that the cross-shelf gradient is smaller. In the Kuroshio area, instead of a warm tongue, the SST contours are turned to be parallel to isobaths during the same period.

[12] To further compare the seasonal migration of the thermal front, positions of the mean (thick white dashed line) and monthly (thick black dashed line) Kuroshio front are depicted in Figure 2. The Kuroshio frontal line is defined as where the local maximal SST gradients in the direction perpendicular to the front are. In general, the mean Kuroshio front is located on the shelf side of the continental slope,

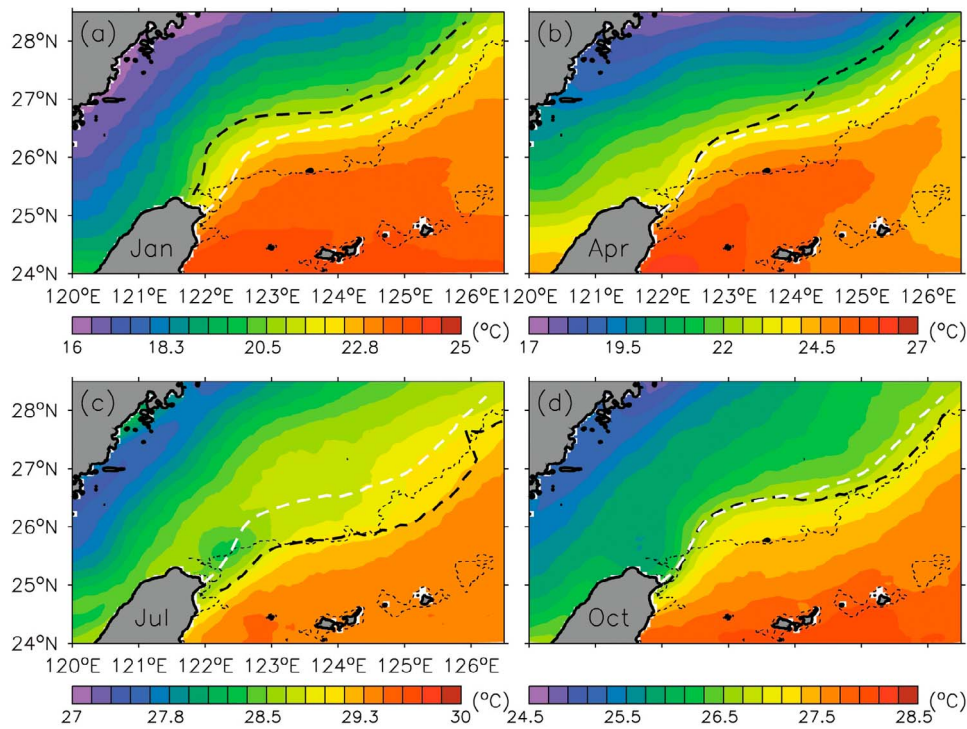


Figure 2. Climatological monthly SST images in (a) January, (b) April, (c) July, and (d) October. Color bar for each month is properly adjusted. The 200 m contour is depicted as thin dashed lines. White thick dashed line is annual mean position of the Kuroshio front, and black thick dashed line indicates the position of the Kuroshio front for each month.

and is parallel to the 200 m isobath except for the northern Taiwan where the front coincides with the isobath. The front tends to be onshore in January and moves offshore by July. In the transition months (April and October), the front almost coincides with the annual mean frontal line.

[13] The Kuroshio front aside, another thermal front is observed in the shelf region. This front often runs in the northeast–southwest direction, except for spring when it shows nearly east–west running (Figure 2b). The seasonality of this front is caused by the interplay between the southward-flowing China Coastal Current and the northward-flowing Taiwan Warm Current. The cold China Coastal Current is strengthened by the northeasterly wind and extends into the Taiwan Strait (Figure 2a). It retreats in spring while the

Taiwan Warm Current strengthens (Figure 2b). In summer, the Taiwan Warm Current becomes stronger and an along-coast cold water band is formed by the coastal upwelling uplifted by the left-bounded current (Figure 2c). This summertime cold water band has been evident by satellite (SST and ocean color images) and shipboard measurements [Tang *et al.*, 2002]. The China Coastal Current (Taiwan Warm Current) tends to be strengthened (weakened) in fall (Figure 2d).

3.2. EOF of SST

[14] Using EOF analysis, the first mode of SST is shown in Figure 3. This mode produces the clear seasonal cycle of SST and explains almost the whole variance (98%). The

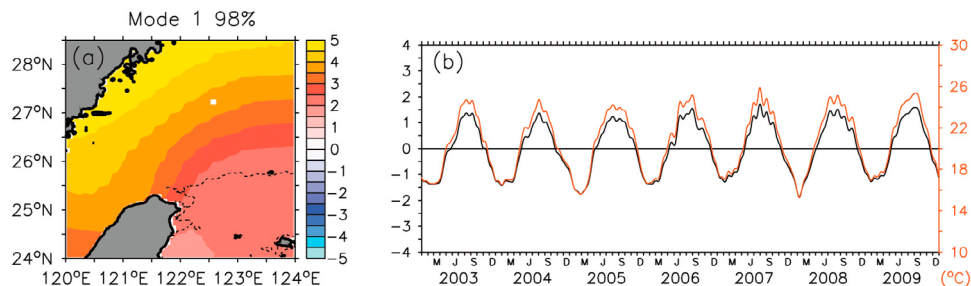


Figure 3. (a) Spatial pattern and (b) time series of the first SST mode. The 200 m contour is depicted as thin dashed line in Figure 3a. The red line in Figure 3b represents the spatial-averaged SST over the entire domain of Figure 3a.

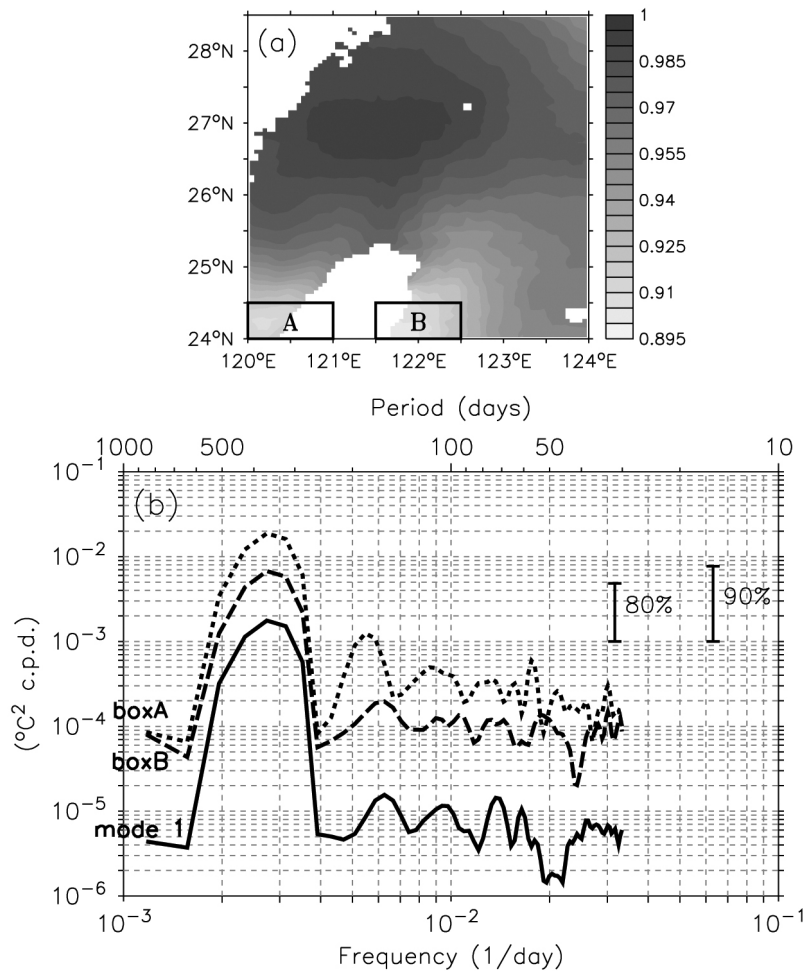


Figure 4. (a) Regression between time series of SST empirical orthogonal function (EOF) mode 1 and SST and (b) spectra of mode 1 (solid line) and SST in boxes A (dotted line) and B (dashed line). The 80% and 90% confidence intervals are depicted.

spatial pattern of this mode exhibits in phase increasing/decreasing of SST over the full analysis' domain. The larger SST increasing occurs during July–September, while the larger SST decreasing is in December–April. The full domain's increasing/decreasing of SST can be straightforwardly attributed to the seasonal variation of heat fluxes into the ocean. The solar radiation heats up (cools down) the SST, and results in the positive (negative) SST anomaly in summer (winter). In addition, cold air outbreaks also obviously contribute the negative anomaly during winter. Expectably, the mode reproduces the spatially averaged SST time series (red line in Figure 3b) in the study region. The correlation between the two curves exceeds 0.99.

[15] When further inspecting the regression between mode 1 and SST time series, their correlation varies spatially (Figure 4a). The higher value centers off northern Taiwan, while the lower value occurs on both coasts of Taiwan. Figure 4b further compares the spectra of time series of mode 1, SST on the east coast (box A in Figure 4a), and west coast (box B) of Taiwan. The most dominant signal among the three time series is the peak at 1 year. Besides the annual signal, not all peaks shown in mode 1 are well present in either box A or box B. For example, the 160 d peak present

in mode 1 is shown in box B, but not in box A where shows a semiannual peak (180 d).

[16] Spatially, the amplitude of the first mode is larger in the shelf region than in the Kuroshio region (Figure 3a). The result can be attributed to that the SST response to heat flux is more sensitive in the shallow shelf region. Although heat flux is nearly homogeneous over the whole region studied, the response can be larger and faster in the shelf region than the Kuroshio region which possesses enormous heat content. Aside from the first mode, the other modes are not significant (variance <2%).

3.3. Spatiotemporal Variability of SSTSI

[17] As mentioned earlier, the Hovmöller diagram of SST cannot distinctly reveal the horizontal movement of the Kuroshio thermal front. The EOF analysis on the SST data resolves only one significant mode related to seasonal heating and cooling. Further investigation deals with SSTSI time series instead. The SSTSI, as described in section 2.1, is obtained by a standardized procedure along sections which are selected to be nearly perpendicular to the strong jet, e.g., the Kuroshio in this study. Figure 5a shows the mean SSTSI pattern (2003–2009) in the fan-shaped area depicted

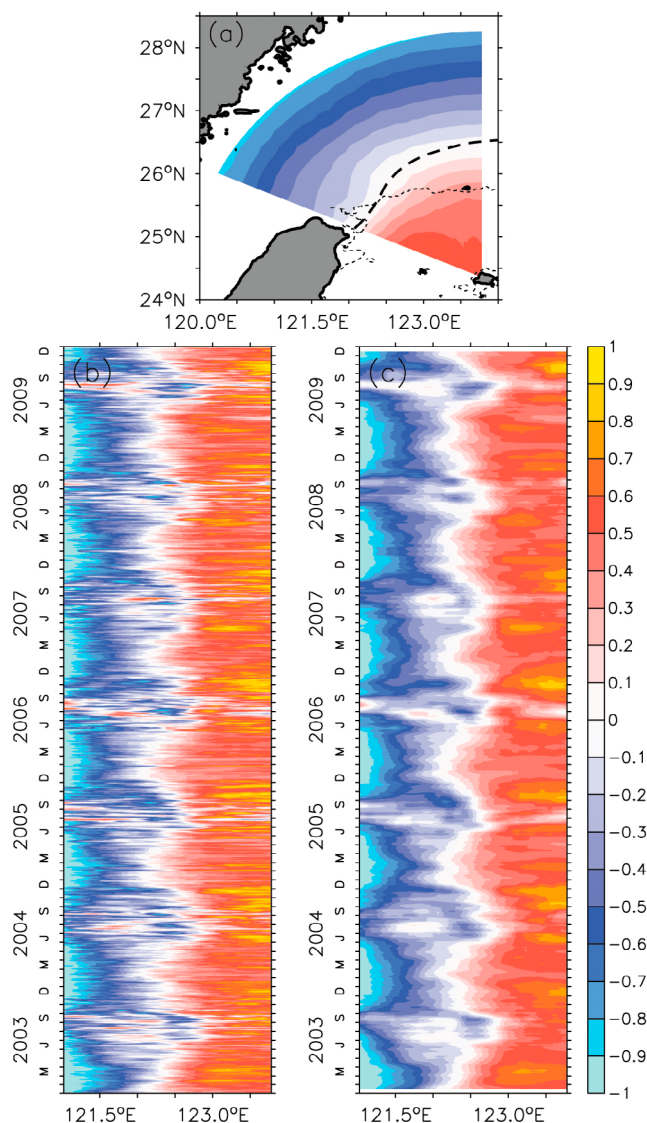


Figure 5. (a) Mean SST standard index (SSTSI) around north Taiwan. Thick dashed line denotes the mean position of the thermal front, and thin dashed line is the 200 m isobath. (b) Hovmöller diagrams of SSTSI along the cross-frontal section (black line in Figure 1a) and (c) its 30 d running average.

as the yellow lines in Figure 1a. The mean SSTSI is positive seaward and negative shoreward, well corresponding to the mean SST pattern in Figure 1a. The largest negative SSTSI takes place along the arc of the fan where the lowest mean SST is observed, while the largest positive value is located around the apex where the warm Kuroshio is prevailing. Within the fan-shaped area, a clear SSTSI border with color in white, whose value is close to zero, runs roughly along the 200 m isobath from the southern boundary (122°E, 25.25°N) to the eastern boundary (123.75°E, 26.5°N). This SSTSI border coincides with the thermal front (dashed line in Figure 5a), indicating that the shift of the SSTSI border can be regarded as the movement of the SST front.

[18] Figures 5b and 5c show the Hovmöller diagram of SSTSI along the same section as Figure 1b and its 30 d running average, respectively. The horizontal movement of SSTSI border with color in white is quite apparent in Figures 5b and 5c. The border fluctuates zonally centered at $\sim 122.5^\circ\text{E}$, from 123°E in summer to 122°E in winter, implying that the seasonal migration of the Kuroshio thermal front. The seasonal shift of the Kuroshio thermal front (or the SSTSI border) agrees well with the published estimates of the seasonal Kuroshio migration [e.g., Sun, 1987; Liang et al., 2003]. A noticeable feature in summer is that the cold water near 200 m isobath ($\sim 122.5^\circ\text{E}$) is wrapped in between two warm waters. The warm water to the east is originated from the Kuroshio, while that to the west comes from the seasonal enhancement of the Taiwan Warm Current originating in the Taiwan Strait [Wu and Hsin, 2005].

3.4. EOF of SSTSI

[19] Besides the seasonal SST variability induced by the surface heat flux difference between summer and winter, more information can be obtained by executing EOF with the SSTSI time series. An EOF analysis is applied to the residual SSTSI, whose temporal mean is removed from the time series. The resolved two leading EOF modes account for 60% and 13% of the total variance, respectively. Figure 6a shows the spatial dependence of the first EOF mode of SSTSI. A clear border serves as a nodal line, which separates large-amplitude oscillations along the arc of the fan-shaped domain and oscillations in the continental slope following the 200 m isobath. The meridional features are out of phase to each other, suggesting that the water in shelf region is getting warmer while it is getting cooler near the slope area. The variance near the apex is tiny. The first SSTSI mode reveals a large-amplitude oscillation around the 200 m isobath (Figure 6a), which has been missing in the EOF analysis of the SST imagery (Figure 3a). The location well coincides with the upwelling in the southern ECS shelf. The upwelling water is seen as a cold dome near the shelf break off northeastern Taiwan, and is potentially important because it provides a major source of nutrients to support primary production in the ECS [e.g., Chen, 1996].

[20] Temporal dependence of the first SSTSI mode shows a significant seasonal variability (Figure 6b). During the northeasterly monsoon period beginning from October to May of the following year, mode 1 coefficient is positive and roughly remains a constant value of about -0.6 . In the other months when the southwesterly wind prevails, the coefficient fluctuates largely between 1.5 and 3.5. The variance in summer is more than 2 times larger than that in winter, showing the contribution of mode 1 is much more significant in summer than winter. This mode takes little effect in the transition months of monsoon (e.g., May and October).

[21] In combined view of both spatial pattern and time series of the first mode, in winter (summer), this SSTSI mode contributes a relative cold (warm) SST to the shelf region and relative warm (cold) SST around the 200 m isobath off northeastern Taiwan. The Kuroshio delivers the warmer water on-shelf, resulting warming over the continental slope in winter. In summer, on the other hand, the Kuroshio axis migrates offshore to the apex of the fan-shaped area, a favorable condition that the cold subsurface water near the slope is capable of upwelling to the

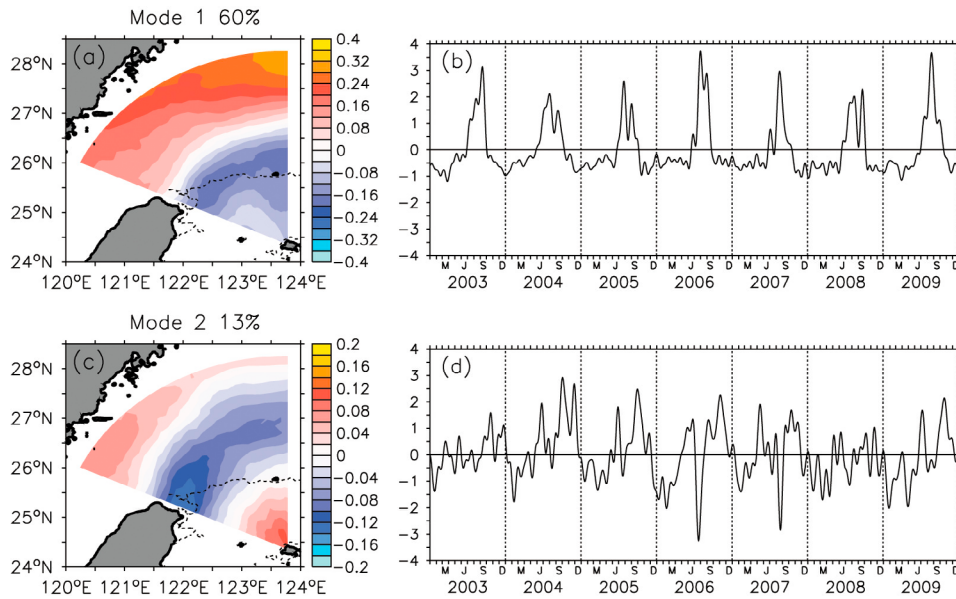


Figure 6. (a, c) Spatial structure and (b, d) temporal variation of two leading SSTSI modes. The 200 m contour is depicted as dashed line in Figures 6a and 6c.

sea surface. Therefore, the negative variance accompanied with the appearance of cold water is generated near the slope in summer. The feature accords with hydrographic and ADCP observations [e.g., Gong *et al.*, 1997; Tang *et al.*, 2000] and a renewed modeling effort [Wu *et al.*, 2008]. On the basis of a high-resolution numerical model simulation, Wu *et al.* [2008] related the surface upwelling to the onshore/offshore migration of the Kuroshio; the onshore movement of the Kuroshio may suppress upwelling of the cold subsurface water.

[22] In the shelf region, mode 1 coefficient is negative between October and May, when the southward advection of the cold China Coastal Current attains its maximum [Lie and Cho, 2002; Isobe, 2008]. Warm waters are confined in the southern Taiwan Strait in winter because the strengthened northeasterly monsoon resists the northward current [Wu *et al.*, 2007]. The cold China Coastal Current water occupies almost the entire shelf region, resulting in a negative SSTSI coefficient. On the other hand, the positive coefficient in summer implies that there should be warm

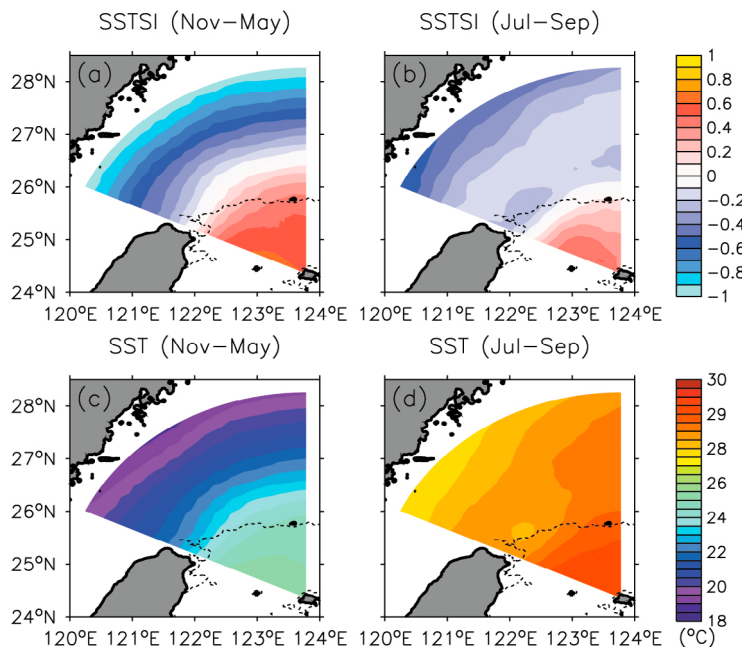


Figure 7. The composite images of SSTS averaged over (a) November–May and (b) July–September. SST composite images averaged over (c) November–May and (d) July–September. The period for average is between 2003 and 2009. The 200 m contour is depicted as dashed line.

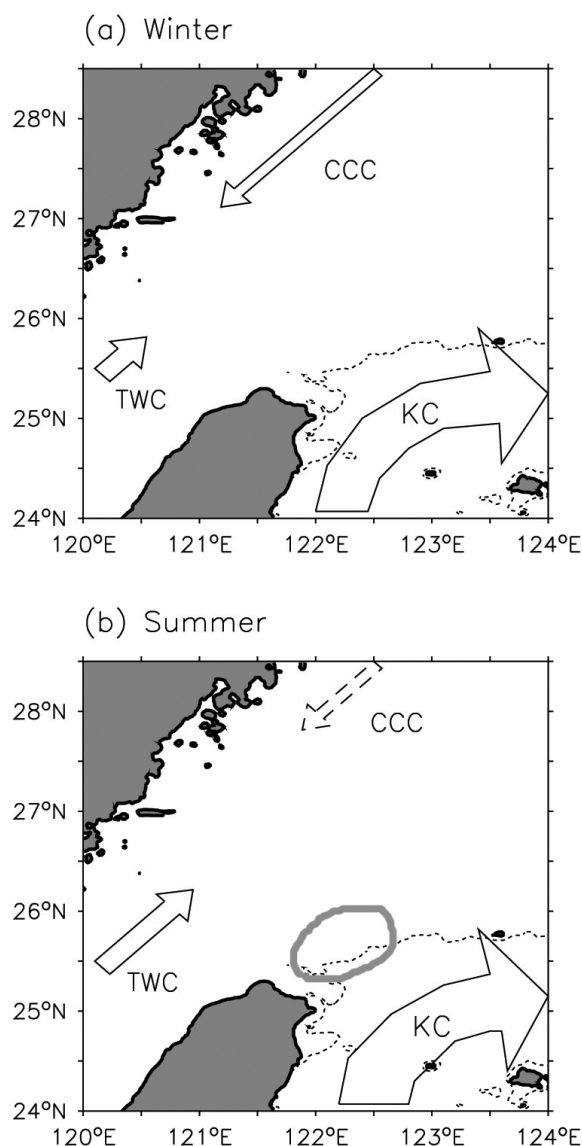


Figure 8. Schemata of the circulation pattern for the Kuroshio (KC), Taiwan Warm Current (TWC), and China Coastal Current (CCC) in (a) winter and (b) summer. Gray circle denotes the cold dome and dashed line shows the 200 m isobath.

waters contributing to the shelf region at the time. Because of the southwesterly monsoon in summer, the downwind Taiwan Warm Current strengthens and increases the northward intrusion of warm waters to the ECS shelf [Wu *et al.*, 2007], resulting in warming in the region. The stronger solar radiation in summer also gives more heat energy into the seas around Taiwan. The seasonal fluctuation aside, year-to-year variations are present in Figure 6b as well.

[23] Further, we compare the composite maps of SSTSI and SST in winter and summer in Figure 7. Both the SSTSI and SST show similar seasonal patterns to the first EOF mode of SSTSI. They reveal a stronger gradient from the shelf region toward the Kuroshio region in winter and a cold dome off northeastern Taiwan in summer. That the SST

gradient is enhanced during wintertime could be resulted from the arrival of the southward-flowing cold China Coastal Current. In summer, the cold dome shows up because of the offshore movement of the Kuroshio, and is isolated by the warm waters from the Kuroshio to the east and Taiwan Warm Current to the west. The water in the shelf region gains heats from the atmosphere and the Taiwan Warm Current, leading a rather homogeneous SST off northern Taiwan.

[24] The seasonality of the SST pattern is closely related to the interplay among the two warm currents (the Kuroshio and Taiwan Warm Current) and the cold China Coastal Current in the region. Figure 8 sketches their circulation pattern during winter and summer. In winter, the northeasterly monsoon strengthened the southward China Coastal Current, which carries more cold water to the southern ECS shelf. Meanwhile, the weakened northward Taiwan Warm Current inputs less warm water. This results in a larger shoreward SST gradient off northern Taiwan. In summer, the shelf region is warmed by the strengthened Taiwan Warm Current and the restrained China Coastal Current, whose existence in summer is still obscure [Isobe, 2008]. Also, the seaward movement of the Kuroshio enables the subsurface cold water to have better opportunity to appear at the sea surface as a cold dome around the continental slope [Wu *et al.*, 2008].

[25] Figures 6c and 6d reveal the spatial pattern and temporal variation of the second SSTSI mode. The mode 2 shows spatially a sandwiched structure with three high-variance centers. The large-amplitude oscillation centered at 122°E, 25.5°N off northern Taiwan extending northeastward is out of phase with oscillations on its both sides, located in the western tip and the apex of the fan-shaped domain, respectively. This mode shows a higher frequency fluctuation than annual signal (Figure 6d).

[26] As mentioned in the Introduction, based on shipboard ADCP, hydrographic observations, and HF radars, several studies suggested that the Kuroshio migration off northeastern Taiwan is seaward in summer and shoreward in winter [e.g., Sun, 1987; Tang *et al.*, 2000; Liang *et al.*, 2003; Ichikawa *et al.*, 2008]. This migration is influenced by the behavior of the upstream Kuroshio off eastern Taiwan. Therefore, we calculate the Kuroshio transport through the ETC using daily sea level anomaly difference between Ishigaki and Genfang (thick solid line in Figure 9a). On the annual time scale, the Kuroshio transport seems to have larger values in summer than winter. This result bears out the summer occurrence of the cold dome off northeastern Taiwan.

[27] Figure 9a further compares the Kuroshio transport with the weekly SSTSI mode 2 time series (thin solid line). When focusing on intraseasonal time scales, both of them have three to five obvious peaks within one year period, indicating that they contain a periodic fluctuation at intervals of 70–120 d. The spectral analyses shown in Figures 10a and 10b support this conclusion. Both spectra have several peaks between 70 and 120 d. This intraseasonal signal is attributed to the interaction between the Kuroshio and westward-propagating mesoscale eddies originating in the interior Pacific [Johns *et al.*, 2001; Hwang *et al.*, 2004; Hsin *et al.*, 2008, 2010]. The weekly AVISO sea level anomalies south of the ETC lend further support (Figure 9b). The

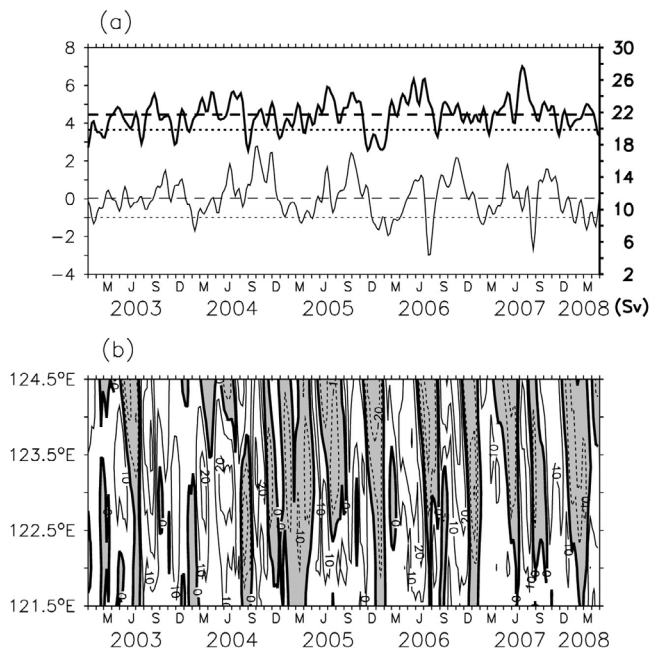


Figure 9. Weekly time series of (a) the second SSTS mode (thin line) and the tidal-gauge-based ETC transport (thick line). The dash lines represent the mean, and the dot lines are 1 standard deviation below the mean. (b) Archiving, Validation, and Interpretation of Satellite Oceanographic data sea level anomalies off eastern Taiwan. The anomalies are averaged over 22–24°N, and the gray shading denotes the negative anomaly.

cyclonic eddies characterized by low sea level anomalies (shading) propagate westward toward the eastern coast of Taiwan. These eddies collide with the Kuroshio at time intervals of 70–120 d, and further influence the flow and temperature in the downstream region off northeastern Taiwan. The local minima of mode 2 coefficient correspond well with the impingement of the cyclonic eddies. The cyclonic eddy decelerates the Kuroshio velocity, and hence the Kuroshio shifts shoreward off northeastern Taiwan. Since the negative peaks in mode 2 coefficient are manifestation of the weakened Kuroshio, the EOF analysis of the innovative SSTS time series is capable of monitoring the Kuroshio transport in the region.

[28] To further examine the relationship between the second mode and the ETC transport in terms of frequency, Figure 10c shows the coherence spectrum between them. Figure 10d gives the corresponding phase angle in which the positive phase angle represents the tidal-gauge-based ETC transport leading the mode time series. They are significantly coherent at two periods of about 45 and 120 d with phase angles of about 90° and 120°, respectively. The result indicates that the ETC transport leads mode 2 at about 11 (40) d for the fluctuation on the period of 45 (120) d. That is, for the 120 d signal, the ETC transport becomes larger (smaller), and sequentially the SSTS becomes positive (negative) with time lag of 40 d because of the offshore (onshore) movement of the Kuroshio. *Ichikawa et al.* [2008] found a similar time lag by satellite altimetry data and sur-

face current derived from HF radars. As discussed above, the westward-propagating mesoscale eddy from the Subtropical Countercurrent (STCC) (~22°N) eddy-rich zone makes the ETC transport and SST off northeastern Taiwan fluctuate at a period of 120 d. In terms of the shorter period fluctuation (45 d), the interaction between the Kuroshio and topography could be the cause of the fluctuation [*Zhang et al.*, 2001; *Hsin et al.*, 2008].

3.5. Interannual Variability of SST in the Southern ECS

[29] As shown in the above sections, interannual variations exist in both the first EOF modes of SST (Figure 3b) and SSTS (Figure 6b). Figures 11a and 11b present the average values of mode 1 coefficients of SST (circle) and SSTS (triangle) in winters and summers of 2003–2009. Here, summer and winter are defined as July–September and January–March, respectively. The averages of SST and SSTS show similar interannual fluctuations regardless of season. Note that SST and SSTS explain different meaning. The SST value represents directly the temperature increasing/decreasing, while the SSTS contrasts the SST pattern between the ECS shelf and the Kuroshio region, the two sides of the thermal front.

[30] In winter, SST has maximum negative value in 2005 and minimum value in 2007. The difference between the two years is ~0.4, indicating that the interannual SST change in the shelf region (where the largest SST value is ~5 in Figure 3a) can reach 2°C. In summer, except for 2003, SST increases year by year from 1.05 in 2004 to 1.42 in 2009. The yearly increasing rate is ~0.07°C on average, indicating that the SST in the shelf region rises by 0.35°C per year from 2004 to 2009. An interesting question is whether this SST rise relates to the global warming? Since the spatial-averaged SST over the entire domain of NGSST (13–63°N, 116–166°E) does not reveal a similar tendency as Figure 11b (figure not shown), the SST rise is proper to attribute to the local effect rather than a long-term climate change. It is the interplay among the two warm currents (Kuroshio and Taiwan Warm Current) and the cold China Coastal Current.

[31] Concerning the SSTS mode 1, wintertime average values range from -0.45 to -0.8. It has larger negative values in 2003 and 2008 and minimum value in 2006. This indicates that the SST in winters of 2003 and 2008 has a larger gradient between the shelf and Kuroshio region than that of 2006. Averaged SSTSs in summer are 1.1–1.8 with larger values in 2003, 2006, and 2009, implying that the cold dome off northern Taiwan is more apparent in the three years.

[32] Figures 12a–12g compare the SST distribution in winters of 2003–2009 to further investigate the interannual change of SST. The mean SST averaged over the seven years is shown in Figure 12h. Demonstrated in Figure 12, three water masses influence the SST pattern in the study region (dashed frame) during winter, the China Coastal Current from the ECS, the Taiwan Warm Current from the Taiwan Strait, and the Kuroshio to the east. Among them, the China Coastal Current is the only cold water source, and it interacts with the Taiwan Warm Current in the northern end of the Taiwan Strait. As the China Coastal Current becomes stronger, it will suppress the Taiwan Warm Current. This can be observed from the position of the 18°C isotherm. The

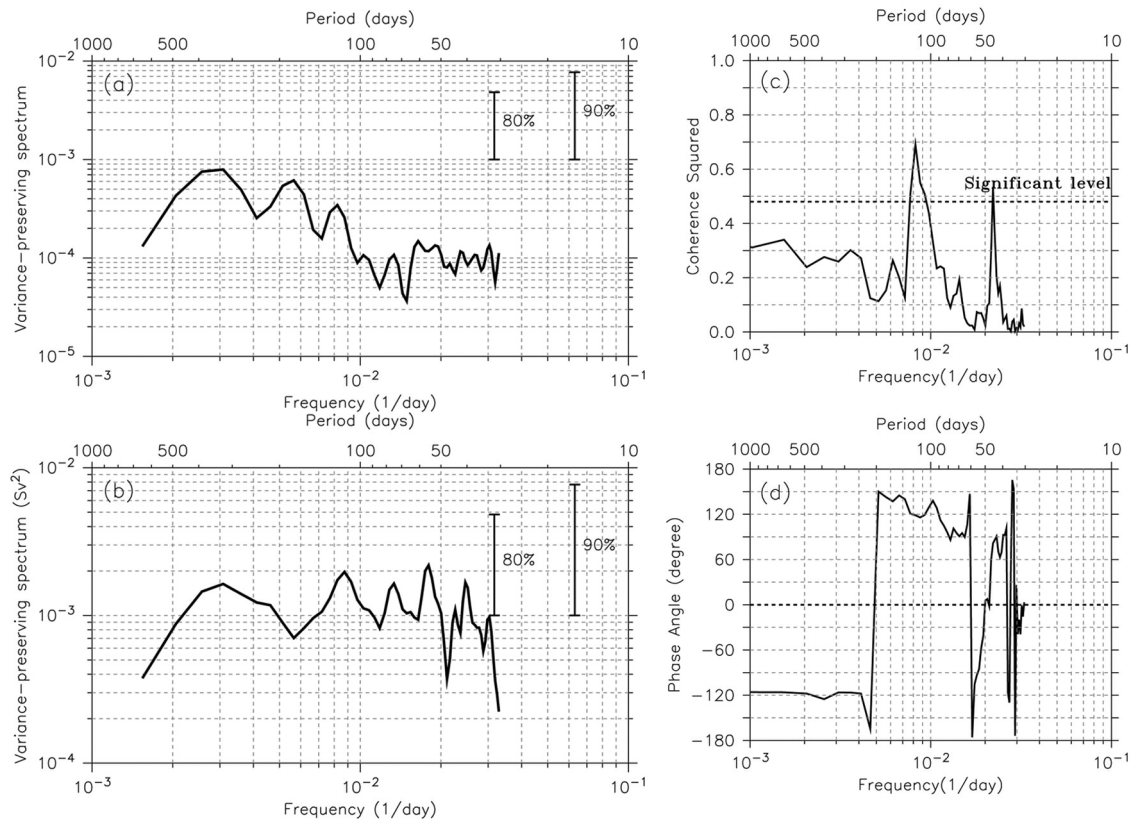


Figure 10. Spectra of (a) SSTSI mode 2 and (b) tidal-gauge-based ETC transport. The 80% and 90% confidence intervals are also depicted. (c) Squared coherence and (d) phase angle of mode 2 and ETC transport. The dotted line denotes the 95% significant level.

18°C isotherm intersects the northwestern coast of Taiwan in 2005 when mode 1 coefficient reaches its minimum of about -1.5 (Figure 10a). On the contrary, the isotherm is confined farther north in 2007 and 2009 when the coefficients are the largest. On the other hand, the warmer water (depicted as the 24°C isotherm) also modulates the SST pattern. The intrusion of the warm Kuroshio tends to increase the SST in the region.

[33] The interannual march of summers from 2003 to 2009 is shown in Figure 13. Unlike the SST during wintertime, the patterns in summer are rather variable. Visually, the temperature goes up from 2004 to 2009, in coincidence with mode 1 coefficients (Figure 11b). The SSTs in the shelf and Kuroshio region are the lowest (highest) in 2004 (2009) when the coefficient reaches its minimum (maximum). One of the most important features in summer, the cold dome near the shelf break, also varies year by year, including its size and location. Among these years, the area of cold dome is more expansive in 2003, 2006, and 2009 when the NINO 3.4 index was positive (>0.5) (http://www.cpc.ncep.noaa.gov/products/analysis_monitoring/ensostuff/ensoyears.shtml). It can be related to the strengthened Kuroshio off northeastern Taiwan in the El Niño years [Hwang and Kao, 2002], which facilitates the appearance of the dome. This result is consistent with the summertime average values of SSTSI mode 1 (triangle in Figure 11b) and reflects the statistical rate of the cold dome occurrence of Cheng *et al.* [2009]. Shown by Cheng *et al.* [2009, Table 1], the cold

dome takes place more frequently in 2003 and 2006 (more than 42 images), while less than 40 images show the dome in 2004, 2005, 2007, and 2008.

[34] Revealed in Figures 12 and 13, SST along the China coast also shows a significant interannual variation. The SST variability is associated with fluctuation of the two coastal currents, which is in turn highly related to the local wind effect. Wu and Hsin [2005] proposed a simple linear equation to evaluate the Taiwan Strait transport by the local wind stress. Wu *et al.* [2007] further suggested that the interannual variation of the Taiwan Strait circulation is influenced by the variability of the wind. Though there was no quantitative study about the wind effect on the China Coastal Current, wind is always regarded as an important factor in the shallow shelf region. We then relate the interannual change of the coastal SST to the winds in winter and summer. Winds in the ECS (ECS wind; 118–128°E, 25–33°N; thin lines) and the Taiwan Strait (TWS wind; 115–123°E, 20–25°N; thick lines) are calculated (Figure 14). Graphically, the ECS wind is dominant in winter while the TWS wind is relatively important in summer. In winter, a stronger (weaker) northerly wind results in a stronger (weaker) southward China Coastal Current and a larger (smaller) cold SST area off northern Taiwan. For example, ECS winds in 2005 and 2008 were stronger among the seven years, and the cold SST area was more expansive (Figures 12c and 12f). In contrast, the cold SST area was the least in 2007 when the ECS wind was the weakest (Figure 12e). Instead of the ECS

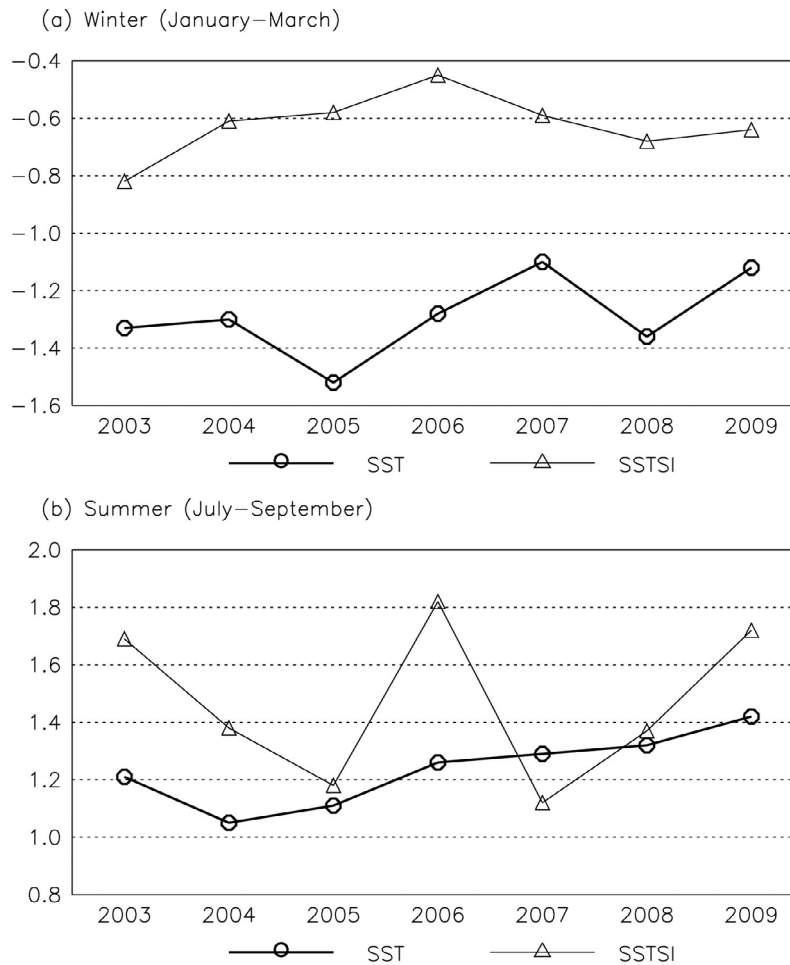


Figure 11. Average values of (a) winters (January–March) and (b) summers (July–September) of 2003–2009 for the first modes of SST (circle) and SSTSI (triangle).

wind, the TWS wind dominates the variation of the coastal SST distribution in summer. As the southerly TWS wind is stronger, the Taiwan Warm Current is also getting stronger. Hence, the stronger Taiwan Warm Current triggers a stronger coastal upwelling, which shows up as a cold water band on the left side of the current. On the other hand, in the years when the TWS wind was weaker (2003, 2006, and 2009), the SST along the coast was higher (Figures 13a, 13d, and 13g). Moreover, the cold SST was the most apparent in 2004 when the TWS wind was the strongest (Figure 13b).

4. Concluding Remarks

[35] This paper implements EOF analyses of a high-resolution SST imagery to investigate the variability of the Kuroshio thermal front off northeastern Taiwan. When EOF is applied directly to the SST data, the first mode accounts for 98% of total variance and represents a seasonal variation. The seasonal migration of the Kuroshio front is well resolved by the SST-based Standardized Index (SSTSI) proposed in this study. The first SSTSI mode accounts for 60% of total variance, and reveals a significant seasonal cycle related to the strong monsoonal winds. A large-amplitude oscillation centered at 122.5°E, 25.5°N in mode 1 coincides

with the upwelling in the southern ECS shelf. The Kuroshio axis migrates seaward in summer, resulting in the occurrence of cold dome favors in summer rather than winter. The results are consistent with ADCP observations and model simulations described in the literature.

[36] The second mode of SSTSI is attributed to the Kuroshio fluctuation in the upstream region east of Taiwan. On the basis of tidal gauge measurements on both sides of ETC, the shoreward (seaward) migration of the thermal front tends to occur when the Kuroshio transport is weaker (larger). The results accord with surface flow patterns derived from HF radars. Both mode 2 and ETC transport fluctuates at periods of ~120 d and ~45 d. The signal with longer period of 120 d is resulted from westward-propagating eddies colliding with the Kuroshio east of Taiwan, while the shorter one is attributed to the Kuroshio instability.

[37] Along the China coast, in winter, the northeasterly wind is dominant in the ECS, which triggers the cold China Coastal Current flowing to the south. On the other hand, the southwesterly wind in the Taiwan Strait, which results in a coastal upwelling on its left side, plays an important role in summer. In addition to seasonal variation, both EOF mode 1 coefficients of SST and SSTSI present interannual varia-

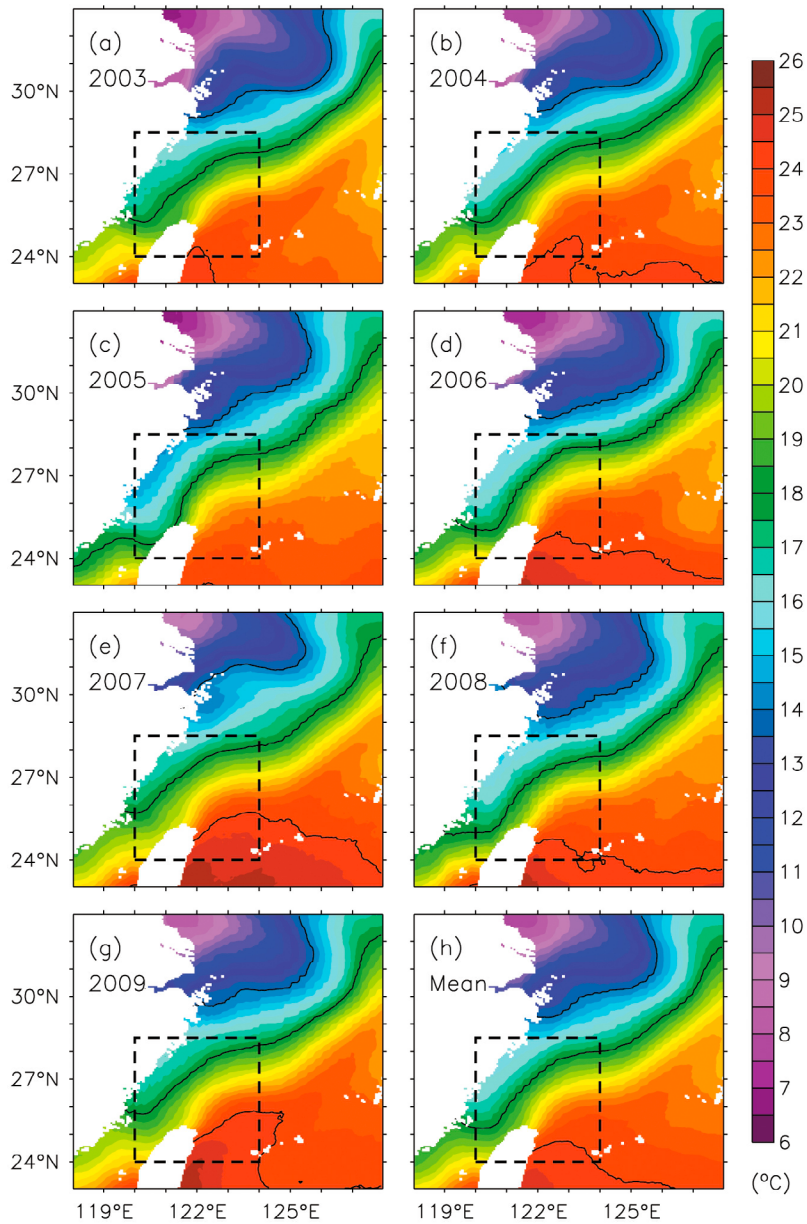


Figure 12. Average SST in winters of 2003–2009. (a–g) Average SST in winters (January–March) of 2003–2009, respectively. (h) Mean SST averaged over the seven years. Black contours denote the 14, 18, and 24°C isotherms. Dashed frame depicts the area for the EOF analysis.

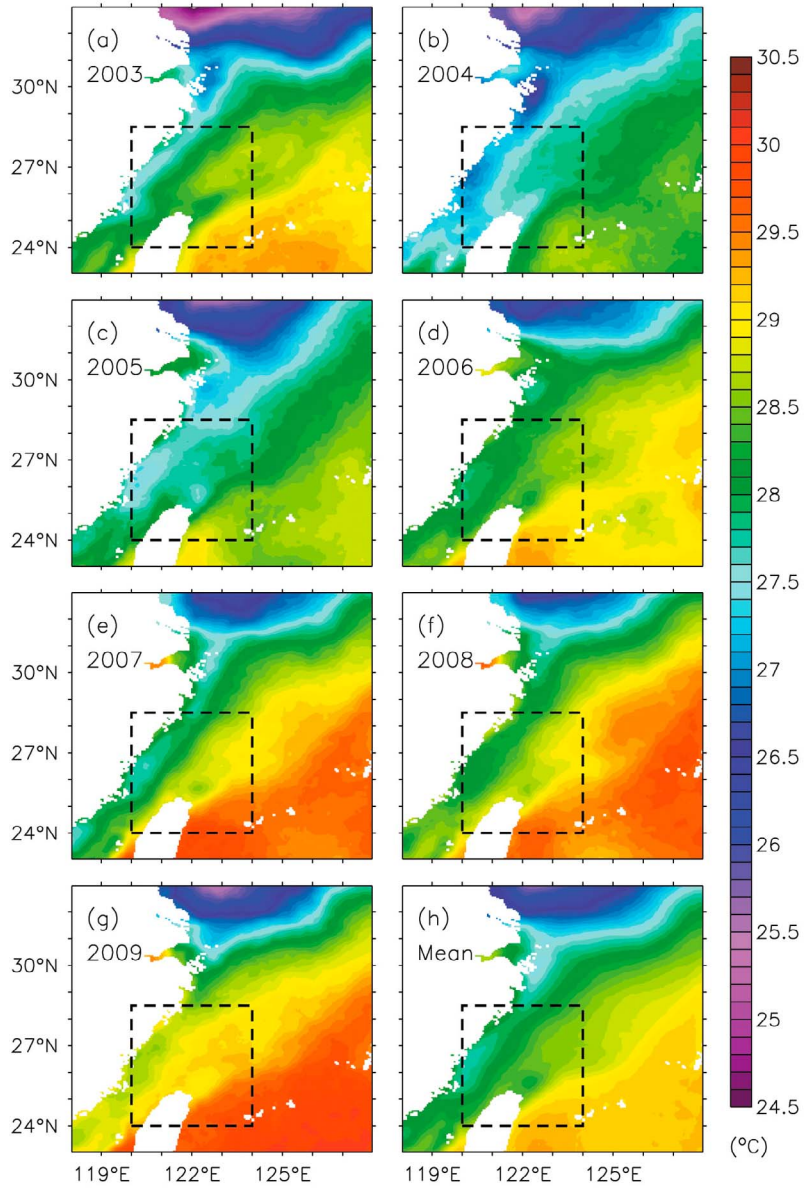


Figure 13. Same as Figure 12 but for summers (July–September).

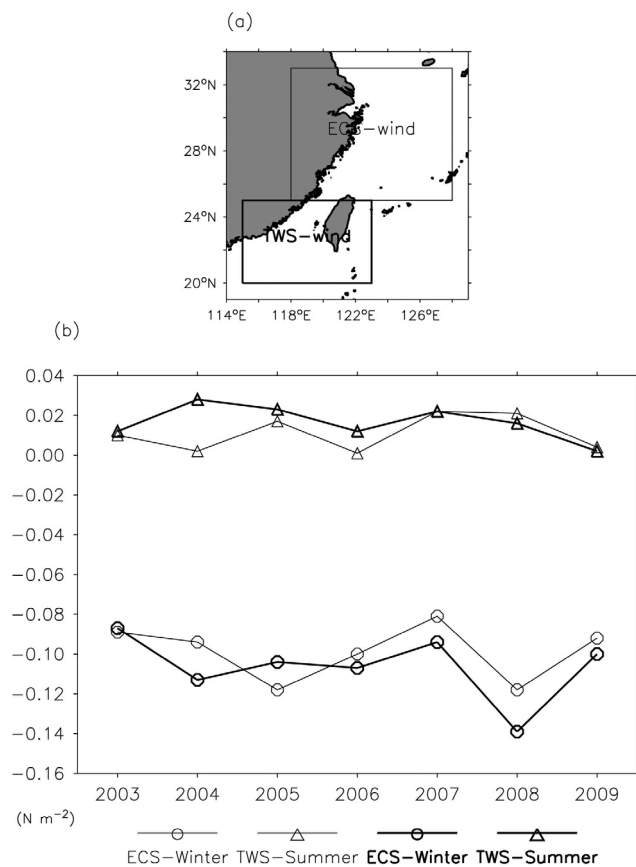


Figure 14. (a) Meridional winds are averaged over the ECS region and the Taiwan Strait (TWS) region. (b) The winds in winter and summer (circle and triangle, respectively).

tions. The year-to-year variation is resulted from the interplay between the Kuroshio, the China Coastal Current, and the Taiwan Warm Current. The Kuroshio off northeastern Taiwan strengthens in the summers of the El Niño years, and hence the area of cold dome is more expansive.

[38] **Acknowledgments.** The authors would like to thank the anonymous reviewer and Igor Belkin for their careful review of the manuscript and detailed suggestions to improve the manuscript. T.-L.C. and C.-R. W. were supported by the National Science Council, Taiwan, under grants NSC 99-2811-M-003-026 and NSC 99-2628-M-003-001.

References

Belkin, I., and P. Cornillon (2003), SST fronts of the Pacific coastal and marginal seas, *Pac. Oceanogr.*, *1*(2), 90–113.

Chao, S.-Y. (1991), Circulation of the East China Sea, a numerical study, *J. Oceanogr.*, *42*, 273–295, doi:10.1007/BF02123503.

Chen, C.-T. A. (1996), The Kuroshio intermediate water is the major source of nutrients on the East China Sea continental shelf, *Oceanol. Acta*, *19*, 523–527.

Chen, C.-T. A. (2009), Chemical and physical fronts in the Bohai, Yellow and East China seas, *J. Mar. Syst.*, *78*(3), 394–410, doi:10.1016/j.jmarsys.2008.11.016.

Cheng, Y.-H., C.-R. Ho, Z.-W. Zheng, Y.-H. Lee, and N.-J. Kuo (2009), An algorithm for cold patch detection in the sea off northeast Taiwan using multi-sensor data, *Sensors*, 5521–5533, doi:10.3390/s90705521.

Chuang, W.-S., and W.-D. Liang (1994), Seasonal variability of intrusion of the Kuroshio water across the continental shelf northeast of Taiwan, *J. Oceanogr.*, *50*, 531–542, doi:10.1007/BF02235422.

Gong, G.-C., F.-K. Shiah, K.-K. Liu, W.-S. Chuang, and J. Chang (1997), Effect of the Kuroshio intrusion on the chlorophyll distribution in the southern East China Sea during spring 1993, *Cont. Shelf Res.*, *17*(1), 79–94, doi:10.1016/0278-4343(96)00022-2.

Hickox, R., I. M. Belkin, P. Cornillon, and Z. Shan (2000), Climatology and seasonal variability of ocean fronts in the East China, Yellow and Bohai seas from satellite SST data, *Geophys. Res. Lett.*, *27*(18), 2945–2948, doi:10.1029/1999GL011223.

Hsin, Y.-C., C.-R. Wu, and P.-T. Shaw (2008), Spatial and temporal variations of the Kuroshio east of Taiwan, 1982–2005: A numerical study, *J. Geophys. Res.*, *113*, C04002, doi:10.1029/2007JC004485.

Hsin, Y.-C., T. Qu, and C.-R. Wu (2010), Intra-seasonal variation of the Kuroshio southeast of Taiwan and its possible forcing mechanism, *Ocean Dyn.*, *60*, 1293–1306, doi:10.1007/s10236-010-0294-2.

Hwang, C., and R. Kao (2002), TOPEX/POSEIDON-derived space-time variations of the Kuroshio Current: Applications of a gravimetric geoid and wavelet analysis, *Geophys. J. Int.*, *151*, 835–847, doi:10.1046/j.1365-246X.2002.01811.x.

Hwang, C., C.-R. Wu, and R. Kao (2004), TOPEX/Poseidon observations of mesoscale eddies over the Subtropical Countercurrent: Kinematic characteristics of an anticyclonic eddy and a cyclonic eddy, *J. Geophys. Res.*, *109*, C08013, doi:10.1029/2003JC002026.

Ichikawa, K., R. Tokeshi, M. Kashima, K. Sato, T. Matsuoka, S. Kojima, and S. Fujii (2008), Kuroshio variations in the upstream region as seen by HF radar and satellite altimetry data, *Int. J. Remote Sens.*, *29*(21), 6417–6426, doi:10.1080/01431160802175454.

Isobe, A. (2008), Recent advances in ocean-circulation research on the Yellow Sea and East China Sea shelves, *J. Oceanogr.*, *64*, 569–584, doi:10.1007/s10872-008-0048-7.

Johns, W. E., T. N. Lee, D. Zhang, R. Zantopp, C.-T. Liu, and Y. Yang (2001), The Kuroshio east of Taiwan: Moored transport observations from the WOCE PCM-1 array, *J. Phys. Oceanogr.*, *31*, 1031–1053, doi:10.1175/1520-0485(2001)031<1031:TKEOTM>2.0.CO;2.

Liang, W.-D., T. Y. Tang, Y.-J. Yang, M.-T. Ko, and W.-S. Chuang (2003), Upper-ocean currents around Taiwan, *Deep Sea Res., Part II*, *50*, 1085–1105, doi:10.1016/S0967-0645(03)00011-0.

Lie, H.-J., and C.-H. Cho (2002), Recent advances in understanding the circulation and hydrography of the East China Sea, *Fish. Oceanogr.*, *11*, 318–328, doi:10.1046/j.1365-2419.2002.00215.x.

Oey, L.-Y., Y.-C. Hsin, and C.-R. Wu (2010), Why does the Kuroshio northeast of Taiwan shift shelfward in winter?, *Ocean Dyn.*, *60*, 413–426, doi:10.1007/s10236-009-0259-5.

Qu, T. (2003), Mixed layer heat balance in the western North Pacific, *J. Geophys. Res.*, *108*(C7), 3242, doi:10.1029/2002JC001536.

Sun, X. (1987), Analysis of the surface path of the Kuroshio in the East China Sea, in *Essays on Investigation of Kuroshio*, edited by X. Sun, pp. 1–14, China Ocean Press, Beijing.

Tang, T. Y., J.-H. Tai, and Y.-J. Yang (2000), The flow pattern north of Taiwan and migration of the Kuroshio, *Cont. Shelf Res.*, *20*, 349–371, doi:10.1016/S0278-4343(99)00076-X.

Tang, D., D. R. Kester, I.-H. Ni, H. Kawamura, and H. Hong (2002), Upwelling in the Taiwan Strait during the summer monsoon detected by satellite and shipboard measurements, *Remote Sens. Environ.*, *83*, 457–471, doi:10.1016/S0034-4257(02)00062-7.

Tseng, C., C. Lin, S. Chen, and C. Shyu (2000), Temporal and spatial variations of sea surface temperature in the East China Sea, *Cont. Shelf Res.*, *20*, 373–387, doi:10.1016/S0278-4343(99)00077-1.

Wu, C.-R., and Y.-C. Hsin (2005), Volume transport through the Taiwan Strait: A numerical study, *Terr. Atmos. Oceanic Sci.*, *16*(2), 377–391.

Wu, C.-R., S.-Y. Chao, and C. Hsu (2007), Transient, seasonal and inter-annual variability of the Taiwan Strait Current, *J. Oceanogr.*, *63*, 821–833, doi:10.1007/s10872-007-0070-1.

Wu, C.-R., H.-F. Lu, and S.-Y. Chao (2008), A numerical study on the formation of upwelling off northeast Taiwan, *J. Geophys. Res.*, *113*, C08025, doi:10.1029/2007JC004697.

Yang, Y., C.-T. Liu, T. N. Lee, W. Johns, H.-W. Li, and M. Koga (2001), Sea surface slope as an estimator the Kuroshio volume transport east of Taiwan, *Geophys. Res. Lett.*, *28*(12), 2461–2464, doi:10.1029/2000GL011709.

Zhang, D., T. N. Lee, W. E. Johns, C.-T. Liu, and R. Zantopp (2001), The Kuroshio east of Taiwan: Modes of variability and relationship to interior ocean mesoscale eddies, *J. Phys. Oceanogr.*, *31*, 1054–1074, doi:10.1175/1520-0485(2001)031<1054:TKEOTM>2.0.CO;2.

T.-L. Chiang, Y.-C. Hsin, and C.-R. Wu, Department of Earth Sciences, National Taiwan Normal University, Taipei, Taiwan. (cwu@ntnu.edu.tw)